IET Power Electronics

Research Article

Clamping diodes failure identification based on the discrete wavelet decomposition of the magnetic near-field

ISSN 1755-4535
Received on 24th July 2018
Revised 10th September 2018
Accepted on 11th January 2019
doi: 10.1049/iet-pel.2018.5043
www.ietdl.org

Ali Lahouar[1] ✉, *Mahmoud Hamouda*[1], *Ibtissem Abari*[1], *Jaleleddine Ben Hadj Slama*[1]

[1]*Laboratory of Advanced Technology and Intelligent Systems, National Engineering School of Sousse, University of Sousse, BP 264, Sousse Erriadh 4023, Tunisia*

✉ *E-mail: ali.lahouar@eniso.rnu.tn*

Abstract: Diagnosis of static power converters for distributed power generation systems and electric machines is nowadays a common concern of researchers interested in the reliability of power electronic systems. The conventional diagnosis approaches such as those based on voltage, current, and flux analysis have already been well developed in recent decades. Recently, it was shown that the magnetic near-field measured above the power converter may carry substantial information about the health state of power components. This study proposes, therefore, a novel non-invasive diagnosis method based on the discrete wavelet decomposition of the near-field metered above a static power converter. It is proved that each faulty component can be identified by its appropriate electromagnetic signature. Accordingly, all faulty cases are easily distinguishable, which makes fault classification possible using very simple tools such as envelope detection. The proposed method is validated through experimental tests carried out on a three-phase three-level neutral point clamped inverter operating with faulty clamping diodes. Its advantages compared to previous diagnosis methods are also discussed.

1 Introduction

Multilevel converters have become the most appropriate topologies for high-power and medium voltage applications. This is because they can be connected directly to a medium voltage distribution network with no need for transformers. They have also many salient advantages compared to conventional two-level inverters, such as lower voltage stress of power semiconductors, better quality of output voltages, reduced dv/dt, reduced filter size etc. Currently, multilevel inverters are utilised in many standard industrial processes such as variable speed drives in marine propulsion and railway traction, utility interface with distributed power generation systems, unified power quality controllers, pumps, gas turbine starter etc. [1, 2]. The neutral point clamped (NPC) converter is nowadays considered among the most popular multilevel topologies since it needs the minimum number of electrolytic capacitors and isolated dc sources.

Due to a large number of power semiconductor devices and drive circuits used in all multilevel converters' topologies and the requirement of interruptible services, the reliability of multilevel converters is nowadays seen as a primary concern. Indeed, power converters remain until now more vulnerable than electrical machines in case of variable speed or wind turbine applications. Their reliability is also far lower than photovoltaic (PV) panels in case of PV energy generation. Many approaches are still under investigation to improve the multilevel converters' performance in terms of efficiency and reliability such as faults prediction, online diagnosis of faults, fault tolerant control, the use of redundant switches etc. [3]. At the components' level, the robustness and reliability of static power converters depend enormously on the health state of semiconductor devices and electrolytic capacitors. It was reported in [4] that ∼30% of faults are caused by capacitors' failures, while the power semiconductors are responsible for 21% of faults. Single failure type of power semiconductor is usually more likely than multiple failures type [5]. Typically, these failures are of two forms: open and short-circuit faults. Short-circuit faults are usually destructive. Fortunately, most gate driver circuits available in the market nowadays are able to detect this type of fault [6, 7]. An immediate shutdown of the converter is therefore mandatory to avoid the destruction of power components. As for open-circuit faults, which cannot be detected by the gate driver circuits, they are usually less destructive and may remain undetected for an undetermined time. However, an open-circuit fault may lead to over-voltages and over-currents in the remaining healthy components [7]. This fault deteriorates also the converter's performance, leading e.g. to a weak torque waveform in case of motor-drive applications or highly distorted grid currents in case of grid-tie converters. Fast and accurate open-circuit fault detection and isolation of the defective component are therefore key operations to prevent fault propagation and additional damages [8].

The open-circuit fault detection methods have been extensively studied in the case of conventional two-level inverters. The diagnosis relies generally on the processing of electrical signals such as pole voltages or load/line currents. Other methods are based on the processing of mechanical signals such as speed or vibration in case of motor drive applications. Some of the methods designed for two-level converters have been extended to fit with the three-level NPC topology. However, the number of research papers interested in open-circuit fault diagnosis of NPC converters remains up to now very limited. In [6], a simple open-circuit fault detection method based on the measurement of pole voltages was proposed. Although the method is fast, it needs additional analogue components and voltage sensors; it is also able to identify only the faulty leg. The average current park's vector technique method was applied in [9] to detect the semiconductor open-circuit fault in an NPC inverter feeding a three-phase induction machine. In [10], the slope method is applied to detect the faulty switch of a back to back NPC converter for wind generation systems. In [10] also, the normalised phase currents are computed to identify faulty transistors and clamping diodes in case of a grid-tie NPC inverter operating at unity input power factor. Moreover, a reactive current component is injected to identify the faulty transistor among the pair of the two upper switches of the same leg. Open switch faults are also detected by analysing the pulse width modulation (PWM) switching signals and the line-to-line voltage levels [11]. The artificial intelligence has also contributed to the diagnosis field, through neural networks [12], neuro-fuzzy systems [13] and support vector machines [14]. Finally, some less known methods are model-based. They make use of observers or estimators in order to generate residuals that are compared to a predefined threshold. A fault is notified once this threshold is surpassed. Model-based methods are successfully implemented in case of two-level [15] and three-level topologies [16]. However, almost all

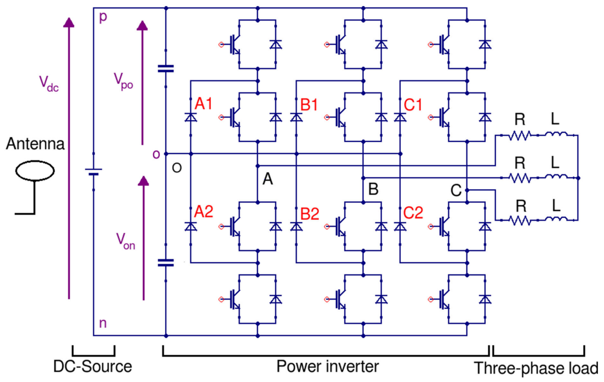

Fig. 1 *Power circuit of a three-phase three-level NPC inverter*

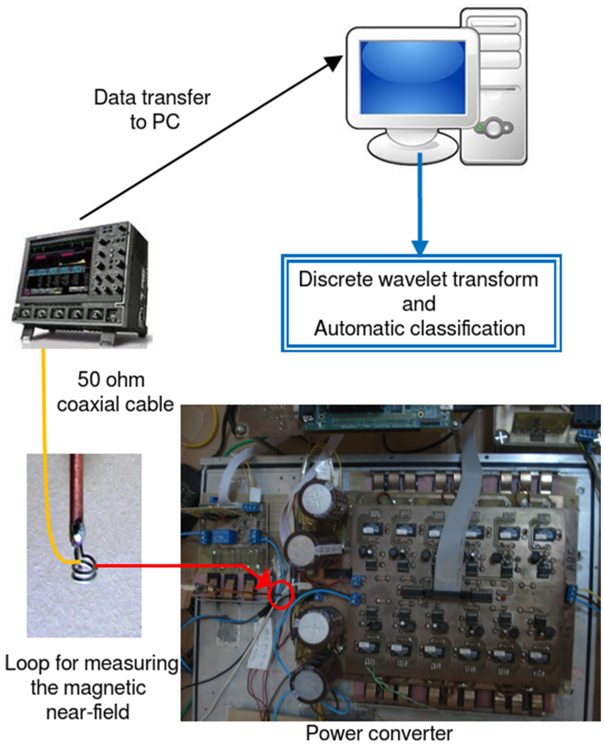

Fig. 2 *Illustrative diagram of test bench utilised for the measurement and processing of the near-field signal*

mentioned methods have ignored the case of low-frequency disturbances, such as highly distorted output current or unbalanced load. Their robustness under these specific conditions is not proved. This is, in particular, the key point from which this study started. The aim is therefore to design a high-frequency (HF) method able to surpass this kind of issue.

Electromagnetic signals are among well-known HF signals. Nevertheless, they are not enough studied in the literature on diagnosis methods, and consequently, they are not fully exploited. Recently, it was shown that the switching operation of PWM converters generates conducted and radiated electromagnetic interferences (EMI), which may carry useful information about the health state of power components [17]. In addition, it is demonstrated that conducted electromagnetic disturbances can effectively be used to identify faulty components [18]. Therefore, it is judicious to make use of EMI in order to detect faults. On the other hand, diode failures are likewise among rarely studied faults. However, they are very important to identify. Diode failures for long periods of time may cause the damage of neighbouring components. In addition, a fault tolerant control may be implemented to cope with diodes' failures. The identification of the faulty diode allows reconfiguring the control algorithm with the aim to ensure an interruptible operation of the converter [19]. Consequently, it is also important to dedicate a complete study for diode faults.

This study proposes a novel identification method of faulty clamping diodes of a three-phase three-level NPC inverter, based on the analysis of the magnetic near-field. The novelty of the method can be explained through the following statements. First and most important, it is a HF method. Therefore, it is immune to low-frequency disturbances, such as unbalanced loads or distorted currents. Second, it makes use of the near-field. Although the near-field has been already processed in previous research, it was not properly addressed and was not the main subject of the study [18]. Third, the proposed approach is non-invasive, which means it does not interfere with the control algorithm, and ensures complete electric isolation between the power stage and the diagnosis system. The idea behind the method is to use the discrete wavelet decomposition to process the near-field metered by a magnetic probe placed above the dc cable of the inverter. The obtained results show that each faulty diode modifies the near-field in a particular and unique way. This specific modification will be called the magnetic signature of the fault. Initially hidden by radiofrequency noise, the near-field signal does not seem to carry any informative data. However, thanks to wavelets, the signature can be easily revealed. Since each signature is unique, a simple classifier based on envelope detection is proposed to identify the faulty diode. This method requires only a shielded magnetic probe to capture the near-field. In addition to non-intrusiveness and electric isolation, such probes are low-cost and can be easily made in laboratories. Furthermore, only one signal is needed to perform the diagnosis, which is the voltage induced across the probe; the image of the near-field.

The remainder of the paper is organised as follows. Section 2 provides a detailed description of the power circuit, the test bench setup and the methodology followed to obtain the electromagnetic signature. Section 3 describes the converter's operation in both healthy and faulty conditions. It explains also the origin of the magnetic signature through theoretical analysis and HF modelling. The processing of obtained results through discrete wavelet decomposition along with fault classification is explained in Section 4. Finally, some concluding remarks are given in Section 5.

2 Power circuit description and test bench setup

The topology of the power converter under study is depicted in Fig. 1. It is a three-phase three-level NPC inverter that consists of 12 power transistors with anti-parallel freewheeling diodes and six clamping diodes. The dc-bus voltage is shared between two capacitors connected in series. Their common connection point is named the dc-bus mid-point O. The inverter is therefore connected to a constant dc source and feeding a three-phase resistor–inductor (RL) load by a controllable three-phase voltage system.

The experimental tests are carried out on a laboratory prototype of a three-level NPC inverter. The power circuit of Fig. 1 is built using 12 metal oxide semiconductor transistors (IRF740) and six clamping diodes (15ETH06). The converter is feeding a three-phase RL load ($R = 20\ \Omega$, $L = 10$ mH). The dc source voltage is set to $V_{dc} = 120$ V. A multi-carrier sinusoidal PWM algorithm is implemented on a digital signal processor (TMS 320F28335). The digital processor provides on its peripheral outputs the appropriate switching pulses, which are routed to the transistors' gates through opto-drivers (HCPL3120). The switching frequency is set to $f_{sw} = 3$ kHz. The output frequency and modulation index of the generated output voltages are set to $f_o = 50$ Hz and $m_o = 0.8$, respectively. A near-field antenna is used to measure the HF emission generated by the inverter. It consists of a 1.5 mm radius probe placed 10 mm above the dc-bus cable and oriented along the z-axis, as illustrated in Fig. 2. This specific location of the antenna has the advantage of being always accessible regardless of whether the inverter is shut-in or not.

For each test with a faulty clamping diode, the electrical connection between the anode and the printed circuit board (PCB) is completely removed to emulate an open-circuit fault. The near-field emitted above the dc-cable induces a voltage across the probe. This voltage, which represents an image of the fault's electromagnetic signature, is fed to the input channel of a digital scope through a 50 Ω coaxial cable. The voltage across the probe is

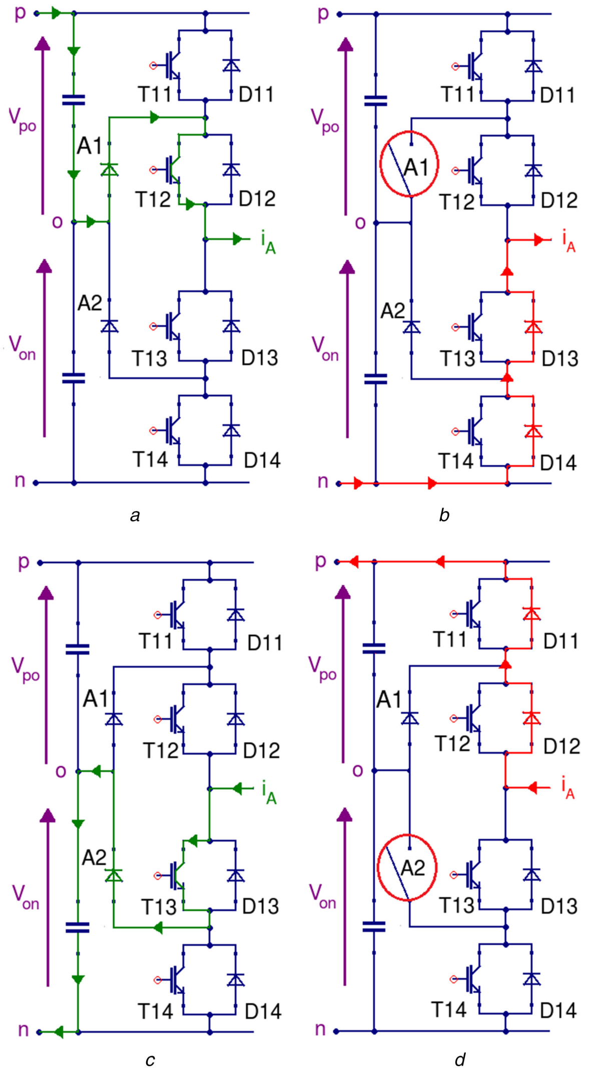

Fig. 3 *Current paths in leg A*
(a) Healthy case with i_A positive, ***(b)*** A1 fault with i_A positive, ***(c)*** Healthy case with i_A negative, ***(d)*** A2 fault with i_A negative

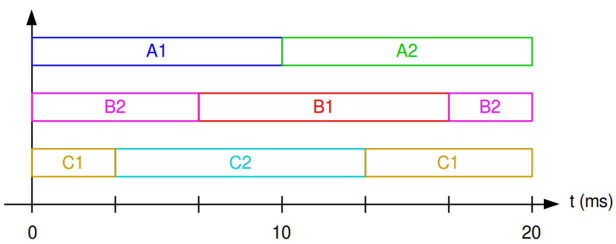

Fig. 4 *Operation regions of the clamping diodes for a 50 Hz fundamental frequency*

measured in steady state and thereafter stored as a data file. The measurement sampling period is set to 2 ns. The obtained data are subsequently transferred to a computer for offline processing. Naturally, the open-circuit fault signature should be 20 ms periodic. Therefore, the HF voltage measurement is performed through a sample window of 20 ms. The HF signal is assumed to be regular within this time interval. The signal is 'regular' if it carries a constant signature that does not evolve through time.

3 Theoretical background

3.1 Converter's operation under normal conditions and faulty clamping diode

For each inverter leg, three switching states exist, namely P, O, and N [19]. The clamping diodes operate only during the switching state O, while the two switches in the middle of the leg are ON. The remaining upper and lower switches are OFF. Therefore, only the state O will be explained in detail in both healthy and faulty modes of operation. Moreover, the analysis assumes that the voltages across the upper and lower capacitors of the dc-bus are equal, i.e. $V_{po} = V_{on} = V_{dc}/2$.

The remainder of the explanation will be restricted to leg A. Two scenarios are considered to explain the effect of faulty clamping diodes on the pole voltage V_{AO}.

Scenario 1: A1 fault with i_A positive.

Assume first, the converter operates in healthy condition and i_A is positive. During the state O, the current flows from the dc source to the load through the clamping diode A1 and the transistor T12, as illustrated in Fig. 3*a*. Accordingly, the pole voltage V_{AO} is equal to zero. In the case of open-circuit fault of A1, the current i_A flows inherently through two freewheeling diodes D13 and D14, as depicted in Fig. 3*b*. The voltage V_{AO} becomes equal to $-V_{dc}/2$ instead of zero. It can, therefore, be concluded that a faulty clamping diode affects the pole voltage waveform in steady state operation. On the other hand, let us consider a transient operation that corresponds e.g. to a commutation from the state P to O. In healthy condition, the pole voltage V_{AO} is switched from $+V_{dc}/2$ to 0. However, in the case of A1 fault, this voltage is switched from $+V_{dc}/2$ to $-V_{dc}/2$. As a consequence, the diode fault affects also the pole voltage slope dV_{AO}/dt. Indeed, the slope is multiplied by two, which inherently will amplify the amplitude of the spectral rails of V_{AO} at the HF range.

Scenario 2: A2 fault with i_A negative.

In healthy condition, the natural path for this current is established through the diode A2 and the transistor T13, as illustrated in Fig. 3*c*. Accordingly, V_{AO} is equal to zero. In case of open-circuit fault of A2, the current path is established through the freewheeling diodes D11 and D12, as shown in Fig. 3*d*. Therefore, the pole voltage V_{AO} becomes equal to $+V_{dc}/2$ instead of zero. Consider also a transient operation that corresponds to a commutation from the state N to O. In healthy condition, V_{AO} is switched from $-V_{dc}/2$ to 0. However, in the case of A2 fault, the slope of V_{AO} is further amplified since the voltage is switched from $-V_{dc}/2$ to $+V_{dc}/2$. Consequently, the A2 fault affects also the steady state and the HF behaviour of the pole voltage, similarly to the A1 fault.

It should be underlined that the difference between the healthy and faulty cases appears in the behaviour of the pole voltage only during the time interval where the faulty diode is supposed to commutate. Indeed, according to the operating principle of the three-level NPC inverter, each clamping diode is supposed to operate during a half-period time interval. Therefore, the switching operation of the diode A1 can occur only within the time interval [0–10] ms, while A2 is able to switch within the time interval [10–20] ms, as shown in Fig. 4.

3.2 Origin and simulation of the magnetic signature

In switching mode power converters, the turn-on and turn-off of power semiconductors are the main cause of EMI as clearly reported in previous research works [20–23]. Indeed, during the switching operation, the parasitic capacitors resonate with the parasitic inductors of the circuit giving rise to transient oscillations. Therefore, HF currents i_H, also referred to conducted disturbances, are created. These currents, flowing through emitting structures of the PCB, create in turn an electromagnetic near-field in the surrounding of the converter [17, 24]. A specific magnetic signature is therefore supposed to appear somewhere inside the frequency spectrum. The signature location within the spectrum depends on the resonance frequency of the circuit, which is usually located between 100 kHz and several MHz [25].

On the other hand, consider a magnetic near-field probe placed above a power cable carrying the current i_H. Therefore, an open-circuit voltage is induced across the probe loop. According to Smith [26], this voltage is proportional to the time derivative of i_H, such that

$$v(t) = M\frac{\mathrm{d}i_{\mathrm{H}}}{\mathrm{d}t}, \quad (1)$$

where M is the mutual inductance between the power cable and the loop of the probe.

A complete and advanced HF modelling is not the aim of this study. Therefore, a simplified equivalent HF circuit is established according to Smith [25]. In addition, neither components' values nor resonance frequencies are calculated since this is not the original purpose of the study. The proposed structure is formed by the association of a variable voltage source connected to a resonant circuit, as illustrated in Fig. 5.

V_{CM} is the common mode voltage expressed as a function of the pole voltages as follows:

$$V_{\mathrm{CM}} = \frac{V_{\mathrm{AO}} + V_{\mathrm{BO}} + V_{\mathrm{CO}}}{3}. \quad (2)$$

L_{p}, R_{p}, and C_{p} are the equivalent parasitic inductance, resistance, and capacitance, respectively. The transfer function in Laplace domain between i_{H} and V_{CM} is, therefore, given as follows:

$$\frac{i_{\mathrm{H}}(s)}{V_{\mathrm{CM}}(s)} = \frac{(1/L_{\mathrm{p}})s}{s^2 + (R_{\mathrm{p}}/L_{\mathrm{p}})s + (1/L_{\mathrm{p}}C_{\mathrm{p}})}, \quad (3)$$

where s is the Laplace operator. The transfer function given in (3) shows that this circuit is behaving in the frequency domain like a band-pass filter. Of course, the bandwidth and resonance frequency depend on the values of parasitic elements.

According to the above discussion, an approximated image of the near-field magnetic signature can be deduced from the waveform of the common mode voltage V_{CM}. Indeed, according to (1) and (3), an image of the voltage across the probe $v(t)$ can be approximated from V_{CM} by applying a band-pass filter followed by a time derivative.

In case of a clamping diode fault, the HF spectrum amplitude of the pole voltage is inherently amplified, as already discussed in Section 3.1. The spectrum amplitude of V_{CM} increases subsequently in the same HF range. Therefore, the amplitude of HF currents is theoretically amplified, leading to a modified near-field magnetic signature, i.e. a different voltage signature across the probe.

To confirm this hypothesis, i.e. faulty diodes cause effectively a modified voltage signature across the probe, computer simulations are carried out. A HF model of a three-level NPC inverter, taking into consideration all parasitic components, is developed and simulated using a circuit-type simulator. Simulations are carried out in healthy, A1 and A2 faulty cases. The sampling period of the simulator is set to 5 ns. The obtained waveforms will be detailed in Section 4.1 in order to put the emphasis on similarities between theoretical and practical results. The simulated waveforms of the processed V_{CM}, after filtering and time derivative, are the expected images of the voltage across the magnetic probe.

4 Experimental results and processing of obtained signals

4.1 Fault detection using discrete wavelet decomposition

The discrete wavelet decomposition is used to extract features from the HF signal. Indeed, the electromagnetic signature is initially hidden and buried by HF noise. Since the resonating circuit is behaving like a band-pass filter, the signature is supposed to appear within a specific frequency band. It is impossible to determine precisely this band without time-frequency tools. Among these tools, the wavelets are the most appropriate, since they are able to delimit the frequency band of the signature by successive filtering and decimating. The signature becomes then more visible in the time domain, which is beneficial for fault classification. To the best of our knowledge, wavelets were not utilised to process the near-field emitted by NPC converters before this work.

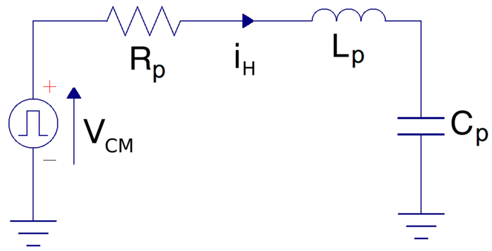

Fig. 5 *Equivalent HF circuit of the converter*

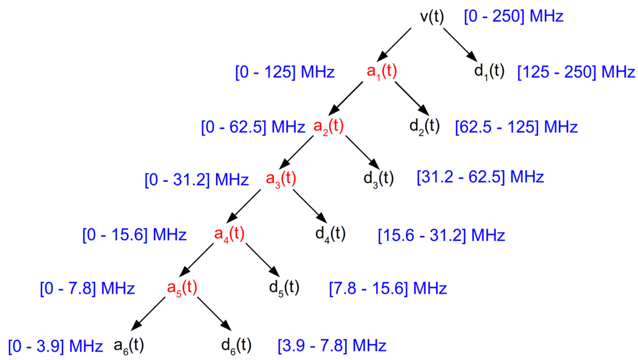

Fig. 6 *Wavelet decomposition tree of* $v(t)$*, and frequency ranges of the obtained signals*

The discrete wavelet transform decomposes the voltage metered across the probe v into one approximation signal (a_n) and n detail signals ($d_1, \ldots, d_n$), where n is the decomposition level, according to

$$v(t) = a_n(t) + d_1(t) + \cdots + d_n(t). \quad (4)$$

In practice, approximation and detail signals are obtained by filtering and decimating (sub-sampling). The original signal $v(t)$ is sampled at 500 MHz (resolution of the oscilloscope). According to the Nyquist–Shannon theorem, the maximum carried frequency is 250 MHz. The frequency ranges of all obtained signals are given in Fig. 6, which represents the wavelet decomposition tree of $v(t)$ until level 6.

Figs. 7*a*–*c* display the approximation signal a_4 of the experimental waveforms of the probe voltage $v(t)$ measured in healthy, A1 fault and A2 fault cases, respectively. The results are obtained with the Coiflet mother function. The a_4 is chosen since the fault signature begins to be distinguishable starting from level 4 of decomposition. Figs. 7*d*–*f* display the expected waveforms of the voltage probe determined according to the theoretical analysis and numerical simulations performed in Section 3.2. These waveforms are obtained in healthy, A1 fault and A2 fault cases. They illustrate the waveforms of V_{CM} after the application of a band-pass filter followed by a first time derivative. The filter bandwidth is set to 0.244–15.6 MHz in order to be consistent with the signal a_4. The similarity between the waveforms obtained with experimental tests and numerical simulations is obvious. The results confirm also the variation of the near-field signature that occurs in case of the faulty clamping diode. The appearance of higher voltage peaks in faulty conditions is then well justified. Therefore, any abnormal variations in pole voltage waveforms due to faulty diodes are reflected in the near-field signature and can be easily detected using an appropriate classifier.

Although a_4 carries an informative signature of the fault, the obtained experimental waveforms in Figs. 7*a*–*c* require further filtering for classification. Therefore, in the remainder of the study, the decomposition will be applied up to the sixth level ($n = 6$) with the aim to obtain cleaner signatures. Consequently, less classification effort will be required to identify the faulty component. Moreover, in addition to Coiflet, the results of decomposition remain almost the same using Haar, Symlet, or Daubechies. Since Haar is the simplest wavelet that needs the minimal real-time computation effort, the approximation signal a_6 will be extracted using this mother function.

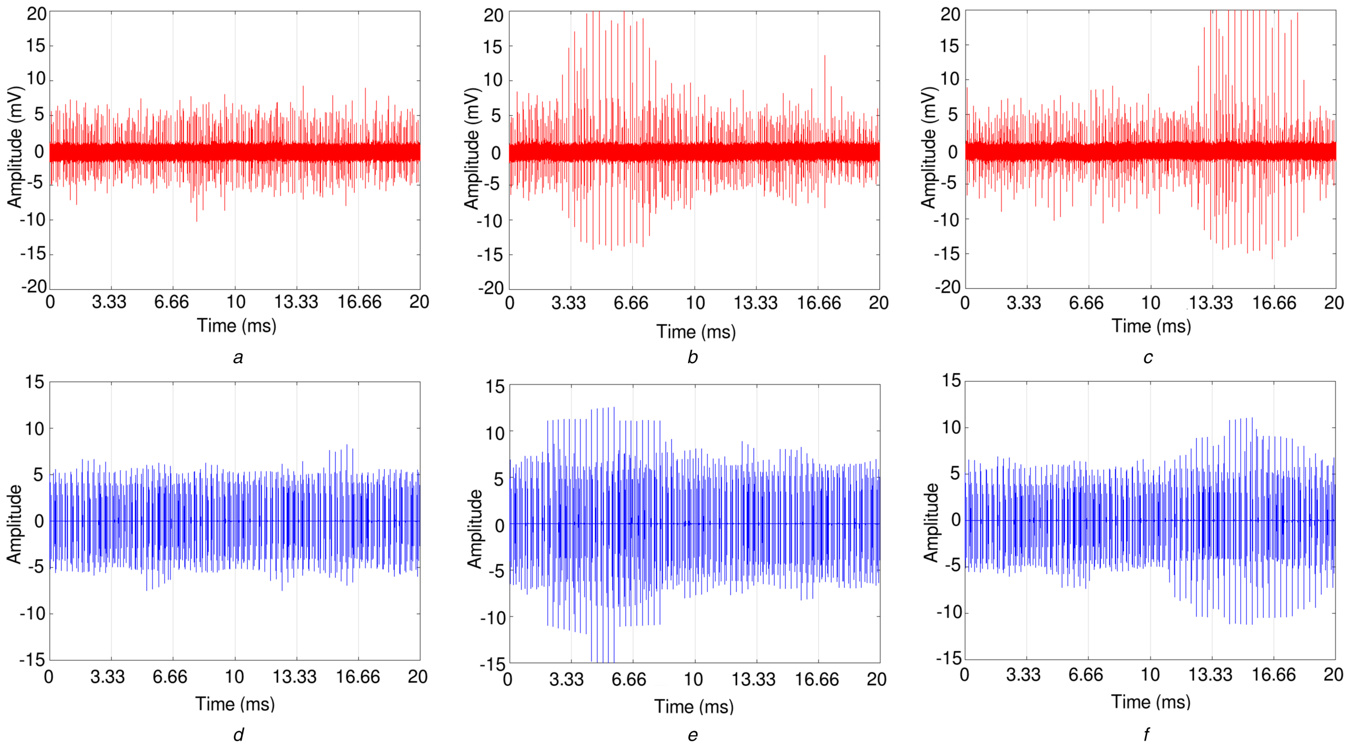

Fig. 7 *Approximation signals a_4 of $v(t)$, obtained with experimental tests*
(a) Healthy case, ***(b)*** Faulty A1 diode, ***(c)*** Faulty A2 diode, derivative of the filtered voltage V_{CM} obtained with numerical simulations, ***(d)*** Healthy case, ***(e)*** Faulty A1 diode, ***(f)*** Faulty A2 diode

Fig. 8 displays the experimental waveforms of the near-field and the approximation signals a_6 obtained under healthy and six faulty cases. The signals a_6 correspond particularly to the frequency band [0–3.9] MHz. In all faulty cases, the signals a_6 include effectively a specific and very clean signature that appears during the time interval in which the faulty diode is supposed to operate. For example, according to Fig. 4, the diode A1 should operate during the first half-period time interval [0–10] ms. In the case of A1 failure, a substantial increase of the amplitude of HF components in a_6 is clearly observed within this time interval. These HF components are now very clear at level 6 (0 to 3.9 MHz), while all remaining frequencies are perfectly filtered. As for the healthy case, it does not contain any HF components at level 6. Hence, the signal a_6 can be used to characterise the health state of the converter. When it does not contain any HF components, the converter is effectively healthy. Otherwise, in case of appearance of any HF components in a_6, their temporal location allows easy identification of the faulty diode.

The magnitude of the signature peaks will drop gradually as the level is increasing until they vanish completely at level 10. Indeed, levels 6 to 10 define the [0.244–3.906] MHz frequency band, which contains the signature. In other words, under 244 kHz, it is impossible to detect the signature. Above 3.9 and up to 15.6 MHz, the signature exists, but it is not recognised easily. Delimiting the appropriate frequency band [0.244–3.906] MHz is the main reason for using wavelets.

4.2 Automatic classification of faults

The fault classification in the previous section was visible to the naked eye, but it cannot be quantified. The main objective of this section is to quantify each defective case in order to automate the classification process. Most HF spikes in each defective case are centred in their corresponding half-period. For example, in the case of A1 which is operating from 0 to 10 ms, most peaks occur between 3.3 and 6.6 ms. Therefore, it is judicious to associate this period of time with A1. Fig. 9 shows this association, where the fundamental period of 20 ms is divided into six equal parts, namely T1, T2,…, T6. Each part is thereafter associated with its corresponding diode that is supposed to cause the HF disturbance at this specific part of the time in case of failure.

In order to characterise each part, a process of envelope detection and energy calculation is applied. Classical envelope detection methods fail in this case since HF spikes are very short and spaced in time. Also calculating energy directly without envelope does not give any result for the same reason. In both cases, the energy will be almost zero. The idea is to dilate the brief peaks if their magnitude is superior to a fixed threshold, so as they remain for longer periods. Therefore, calculating energy by integration with respect to time will not give null values. Contrariwise, it will give important values only when high peaks are present. The following digital signal processing algorithm is then proposed, where x is the envelope discrete signal containing k samples, and r is a resolution coefficient (Fig. 10).

This algorithm is applied offline. The coefficient r is set to 4. The more this coefficient is large, the more the envelope is tight. On the other hand, a small value of this coefficient leads to more dilated HF spikes. This dilatation causes, in turn, the energy of the envelope to become important only when HF peaks are present. Applying this algorithm to the signal a_6 in case of faulty A1 leads to the results shown in Fig. 11. As can be seen, the envelope curve shows dilated peaks at T2. Obviously, the energy of the envelope signal at T2 is greater than its energy anywhere else over [0–20] ms. Since T2 has already been associated with the faulty diode A1 case as illustrated in Fig. 9, the effectiveness and correctness of the proposed classification method are confirmed.

The energy of the envelope is computed as follows:

$$E_x = \sum_{i=1}^{k} |x(i)|^2 . \tag{5}$$

Table 1 shows the obtained energy values of the envelope from T1 to T6 for the seven operating cases. The maximum energy in each case is highlighted with grey colour. It is also clear that the maximum energy corresponds perfectly to the part associated with the faulty diode. The general approach for detecting diode faults is then defined as follows. A diode failure is notified whenever an energy value is greater than a predefined threshold, which may be determined empirically. Then, the maximum energy among T1,...,

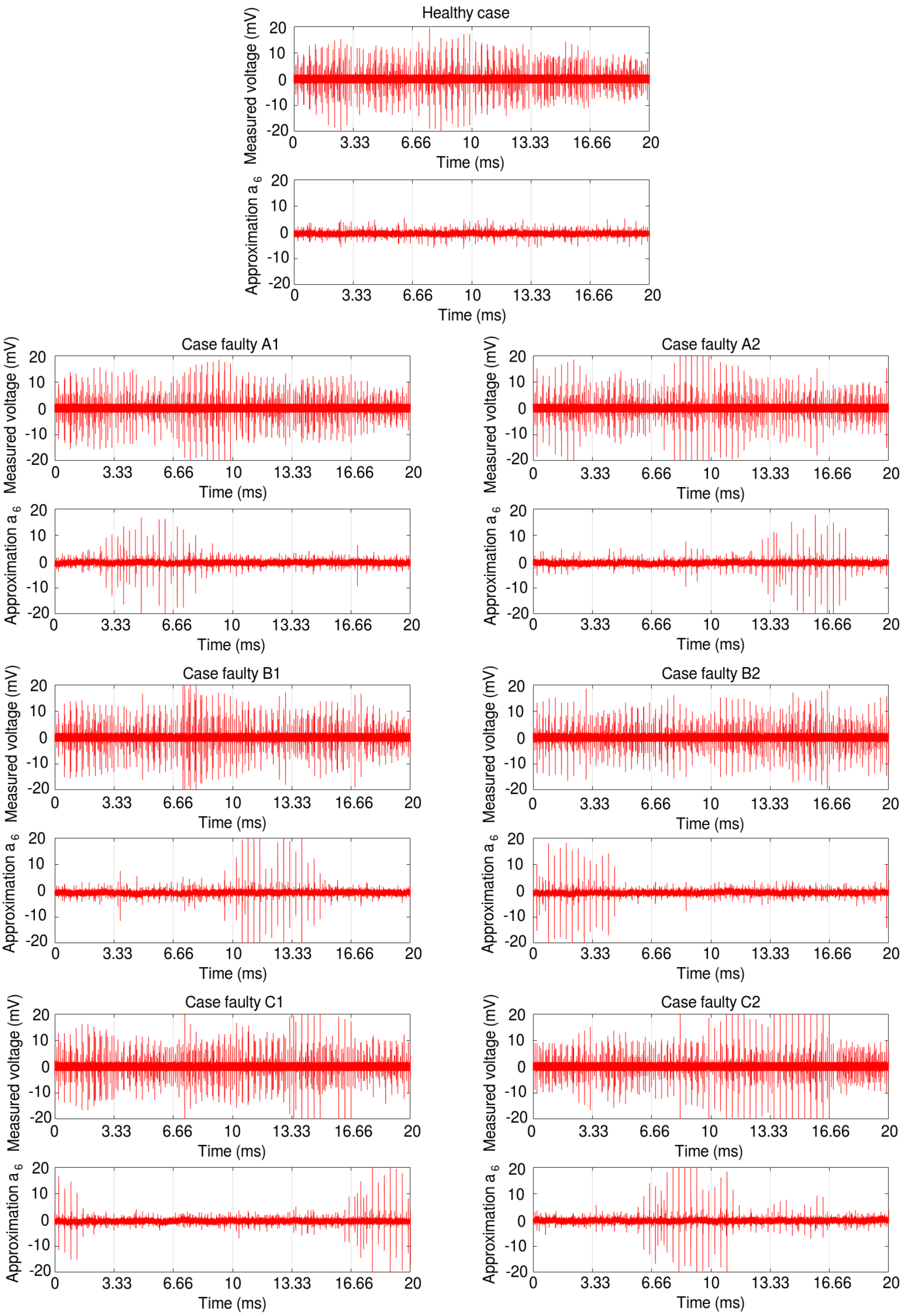

Fig. 8 *Experimental waveforms of the near-field (figures in the top) and the approximated signals a_6 obtained with Haar wavelet (figures in the bottom) in healthy and six faulty cases*

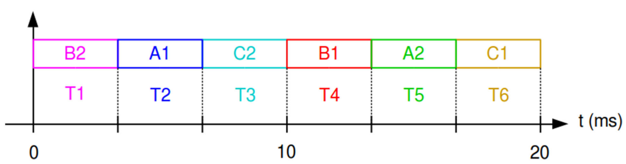

Fig. 9 *Association of defective diodes with specific temporal locations*

T6 is selected. Finally, the associations of Fig. 9 should identify the faulty diode.

4.3 Comparison with conventional methods

The proposed approach has the following advantages with respect to current/voltage-based diagnosis methods:

- The conventional detection methods based on current/voltage analysis [27] are vulnerable to low-frequency disturbances. Indeed, any distortion may be interpreted by the diagnostic system as a fault affecting the inverter [28]. Consequently, a false alarm may be notified. On the other hand, high frequencies are not affected by this kind of issue. The idea is therefore to search a 'HF image' of the fault, which is the main novelty of this work.
- It is non-invasive. Placing a magnetic probe 10 mm above the dc cable is enough to point out any defective clamping diode. The non-intrusiveness is quite useful when dealing with shut-in inverters whose control stages are not accessible. The diagnosis system does neither interfere with the control algorithm nor require additional current/voltage sensors (such as [19, 29]).
- It isolates the diagnosis system from power stages. Unlike current/voltage probes [30], magnetic sensors are not exposed to current or voltage stress. Therefore, they are more reliable and less vulnerable to aging problems. Besides, any destructive fault at the power stage will not affect the diagnosis system.
- Only one signal is required for the analysis. The magnetic near-field involves all the information useful to diagnose the converter health state. However, conventional methods make use of several signals generated by at least three voltage or current sensors.

```
x ← absolute(a6);
M ← max(x)/r;
N ← max(x)/r;
for i from 1 to k
   if x(i) > M
      N ← x(i);
   end;
   if x(i) < N
      x(i) ← N;
   end;
end;
x ← x-M;
```

Fig. 10 *Digital signal processing algorithm*

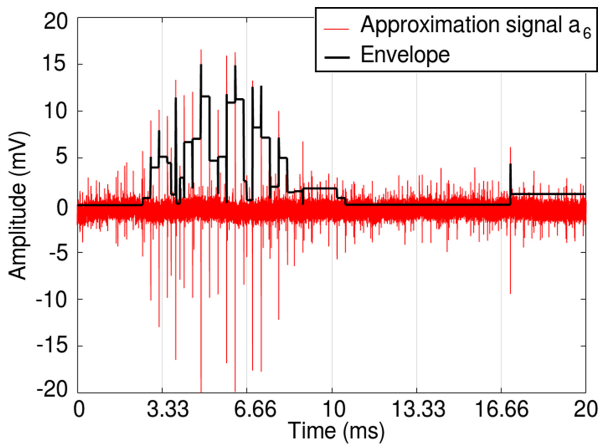

Fig. 11 *Envelope detection of the approximation signal a_6, case of faulty diode A1*

- Magnetic probes are cheap and easy to manufacture, contrary to current and voltage probes. They can be easily built in laboratories. Therefore, there is no problem with the 'additional sensor' in the setup, since this sensor is not costly.

In order to prove the immunity of the proposed approach to low-frequency disturbances, two additional tests are performed. The former is the case of unbalanced load, and the latter is the case of small output currents, both carried out in healthy and faulty diode A1 cases. To make the load unbalanced, the resistance has been changed from 20 to 10 Ω only in phase A. Notice that most detection methods based on current signature assume the three-phase system to be balanced [19]. The effectiveness of the current-based method under the unbalanced system is therefore not proved. The electromagnetic signature, however, is always visible even with an unbalanced load when a fault occurs in diode A1, as shown in Fig. 12*a*. Under healthy conditions, the processed near-field voltage remains the same either with a balanced or unbalanced load. There is, therefore, no risk of false alarm. The second experiment highlights the case of small output currents, where the resistance in all phases is set to 45 Ω. Under such conditions and in the presence of a fault in A1, the current signature becomes ambiguous because of high distortion with respect to amplitude [31]. Nevertheless, the electromagnetic signature is still visible, as shown in Fig. 12*b*. Although its spikes are not high, they are sufficient to perform an accurate classification. As a consequence, even in the presence of low-frequency disturbances or distortions, the electromagnetic signature is always present and visible. It is, therefore, a robust and reliable method that proves its effectiveness under different circumstances.

5 Conclusion

To ensure the fault tolerant operation of a three-level NPC inverter in case of clamping diodes' failure, it is mandatory to identify the faulty component so as to ensure the correct operation of the fault-tolerant algorithm. This study proposed an advanced diagnosis and identification method based on the measurement of the HF magnetic near-field emitted by an NPC inverter. The obtained signals in both healthy and faulty cases are processed using the discrete wavelet decomposition along with envelope detection and energy calculation. This method permitted to get an informative signature that can characterise the healthy and every faulty case, by pointing out the faulty diode. The proposed approach has the following advantages: (i) the measurement method of the HF near-field is non-invasive. Moreover, HF signals are not affected by low-frequency disturbances. (ii) It isolates the diagnosis system from the power stage and does not interfere with the control algorithm. It avoids also the use of additional costly current/voltage sensors. The future work involves the detection and classification of electromagnetic signatures in case of faulty transistors, as well as the development of real-time fault diagnosis solutions based on the analysis of magnetic near-field.

Table 1 Energy of the envelope during the six parts in the healthy and faulty cases (values multiplied by 1000)

	Healthy	Case A1	Case A2	Case B1	Case B2	Case C1	Case C2
T1	0.4941	8.4321	0.3742	0	236.4818	80.3610	0
T2	1.7026	188.4996	0.0068	48.1152	85.9533	0.5871	6.9960
T3	2.1331	56.0367	12.2852	10.7237	31.2030	0.5871	512.0414
T4	2.4511	0.8749	8.9641	389.4531	16.4216	3.5324	132.7541
T5	0.4908	0.0067	116.2889	125.1911	16.4216	5.5381	14.7001
T6	1.2615	4.1832	79.8095	34.9810	10.1555	329.7464	0.0029

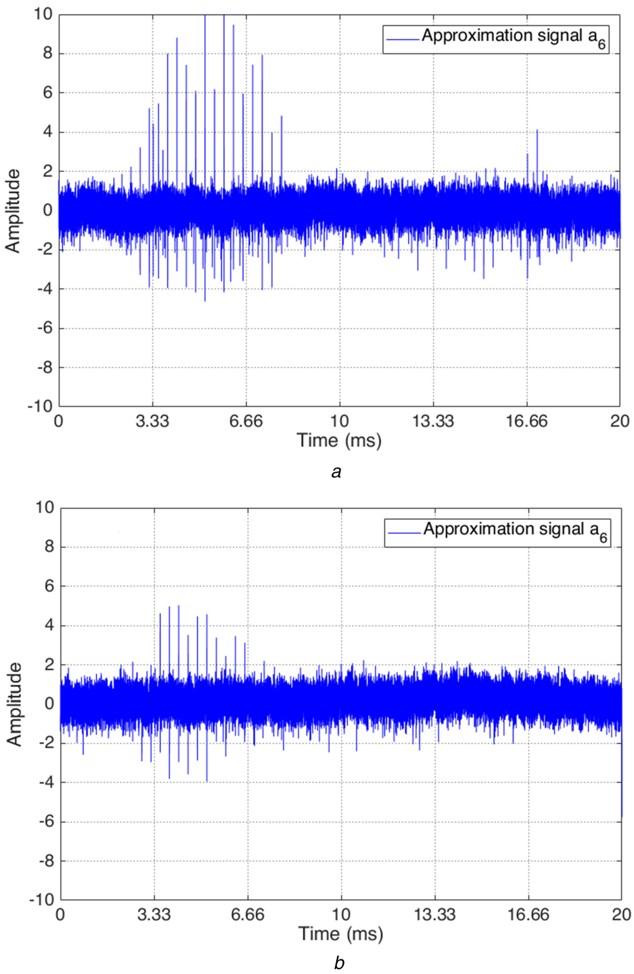

Fig. 12 *Approximation signals a_6 of $v(t)$, obtained with Coiflet wavelet, in the presence of a fault in diode A1, in case of*
(a) Unbalanced load, ***(b)*** Small output currents

6 References

[1] Kouro, S., Malinowski, M., Gopakumar, K., *et al.*: 'Recent advances and industrial applications of multilevel converters', *IEEE Trans. Ind. Electron.*, 2010, **57**, (8), pp. 2553–2580

[2] Abu-Rub, H., Bayhan, S., Moinoddin, S., *et al.*: 'Medium-voltage drives: challenges and existing technology', *IEEE Power Electron. Mag.*, 2016, **3**, (2), pp. 29–41

[3] Song, Y., Wang, B.: 'Survey on reliability of power electronic systems', *IEEE Trans. Power Electron.*, 2013, **28**, (1), pp. 591–604

[4] Wang, H., Liserre, M., Blaabjerg, F.: 'Toward reliable power electronics: challenges, design tools, and opportunities', *IEEE Ind. Electron. Mag.*, 2013, **7**, (2), pp. 17–26

[5] Murphey, Y.L., Masrur, M.A., Chen, Z., *et al.*: 'Model-based fault diagnosis in electric drives using machine learning', *IEEE/ASME Trans. Mechatronics*, 2006, **11**, (3), pp. 290–303

[6] Kim, T.J., Lee, W.C., Hyun, D.S.: 'Detection method for open-circuit fault in neutral-point-clamped inverter systems', *IEEE Trans. Ind. Electron.*, 2009, **56**, (7), pp. 2754–2763

[7] Li, B., Shi, S., Wang, B., *et al.*: 'Fault diagnosis and tolerant control of single IGBT open-circuit failure in modular multilevel converters', *IEEE Trans. Power Electron.*, 2016, **31**, (4), pp. 3165–3176

[8] Haghnazari, S., Khodabandeh, M., Zolghadri, M.R.: 'Fast fault detection method for modular multilevel converter semiconductor power switches', *IET Power Electron.*, 2016, **9**, (2), pp. 165–174

[9] Mendes, A.M.S., Abadi, M.B., Cruz, S.M.A.: 'Fault diagnostic algorithm for three level neutral point clamped ac motor drives, based on the average current park's vector', *IET Power Electron.*, 2014, **7**, (5), pp. 1127–1137

[10] Lee, J.S., Lee, K.B., Blaabjerg, F.: 'Open-switch fault detection method of a back-to-back converter using NPC topology for wind turbine systems', *IEEE Trans. Ind. Appl.*, 2015, **51**, (1), pp. 325–335

[11] Trabelsi, M., Boussak, M., Gossa, M.: 'PWM-switching pattern-based diagnosis scheme for single and multiple open-switch damages in VSI-fed induction motor drives', *ISA Trans.*, 2012, **51**, (2), pp. 333–344

[12] Masrur, M.A., Chen, Z., Murphey, Y.: 'Intelligent diagnosis of open and short circuit faults in electric drive inverters for real-time applications', *IET Power Electron.*, 2010, **3**, (2), pp. 279–291

[13] Awadallah, M.A., Morcos, M.M.: 'Automatic diagnosis and location of open switch fault in brushless dc motor drives using wavelets and neuro-fuzzy systems', *IEEE Trans. Energy Convers.*, 2006, **21**, (1), pp. 104–111

[14] Wang, T., Qi, J., Xu, H., *et al.*: 'Fault diagnosis method based on FFT-RPCA-SVM for cascaded-multilevel inverter', *ISA Trans.*, 2016, **60**, pp. 156–163

[15] Gou, B., Ge, X., Wang, S., *et al.*: 'An open-switch fault diagnosis method for single-phase PWM rectifier using a model-based approach in high-speed railway electrical traction drive system', *IEEE Trans. Power Electron.*, 2016, **31**, (5), pp. 3816–3826

[16] Ge, X., Pu, J., Gou, B., *et al.*: 'An open-circuit fault diagnosis approach for single-phase three-level neutral-point-clamped converters', *IEEE Trans. Power Electron.*, 2018, **33**, (3), pp. 2559–2570

[17] Chen, Y., Pei, X., Nie, S., *et al.*: 'Monitoring and diagnosis for the dc–dc converter using the magnetic near field waveform', *IEEE Trans. Ind. Electron.*, 2011, **58**, (5), pp. 1634–1647

[18] Abari, I., Lahouar, A., Hamouda, M., *et al.*: 'Fault detection methods for three-level NPC inverter based on dc-bus electromagnetic signatures', *IEEE Trans. Ind. Electron.*, 2018, **65**, (7), pp. 5224–5236

[19] Choi, U.M., Lee, J.S., Blaabjerg, F., *et al.*: 'Open-circuit fault diagnosis and fault-tolerant control for a grid-connected NPC inverter', *IEEE Trans. Power Electron.*, 2016, **31**, (10), pp. 7234–7247

[20] Dutta, A., Ang, S.S.: 'Electromagnetic interference simulations for wide-bandgap power electronic modules', *IEEE J. Emerging Sel. Topics Power Electron.*, 2016, **4**, (3), pp. 757–766

[21] Middelstaedt, L., Lindemann, A.: 'Methodology for analysing radiated EMI characteristics using transient time domain measurements', *IET Power Electron.*, 2016, **9**, (10), pp. 2013–2018

[22] Beghou, L., Costa, F., Pichon, L.: 'Detection of electromagnetic radiations sources at the switching time scale using an inverse problem-based resolution method – application to power electronic circuits', *IEEE Trans. Electromagn. Compat.*, 2015, **57**, (1), pp. 52–60

[23] Benyoubi, F., Pichon, L., Bensetti, M., *et al.*: 'An efficient method for modeling the magnetic field emissions of power electronic equipment from magnetic near field measurements', *IEEE Trans. Electromagn. Compat.*, 2017, **59**, (2), pp. 609–617

[24] Chen, Y., Nie, S., Pei, X., *et al.*: 'State monitoring and fault diagnosis of the PWM converter using the magnetic field near the inductor components'. 2010 IEEE Energy Conversion Congress and Exposition, Atlanta, GA, USA, 2010, pp. 1901–1907

[25] Ogasawara, S., Akagi, H.: 'Modeling and damping of high-frequency leakage currents in PWM inverter-fed ac motor drive systems', *IEEE Trans. Ind. Appl.*, 1996, **32**, (5), pp. 1105–1114

[26] Smith, D.C.: '*High frequency measurements and noise in electronic circuits*' (Springer, USA, 1992)

[27] Rothenhagen, K., Fuchs, F.W.: 'Performance of diagnosis methods for IGBT open circuit faults in voltage source active rectifiers'. 2004 IEEE 35th Annual Power Electronics Specialists Conf. (IEEE Cat No. 04CH37551), Aachen, Germany, 2004, vol. 6, pp. 4348–4354

[28] Peuget, R., Courtine, S., Rognon, J.: 'Fault detection and isolation on a PWM inverter by knowledge-based model', *IEEE Trans. Ind. Appl.*, 1998, **34**, (6), pp. 1318–1326

[29] Lamb, J., Mirafzal, B.: 'Open-circuit IGBT fault detection and location isolation for cascaded multilevel converters', *IEEE Trans. Ind. Electron.*, 2017, **64**, (6), pp. 4846–4856

[30] Farnesi, S., Fazio, P., Marchesoni, M.: 'A new fault tolerant NPC converter system for high power induction motor drives'. 8th IEEE Symp. on Diagnostics for Electrical Machines, Power Electronics Drives, Bologna, Italy, 2011, pp. 337–343

[31] Lu, B., Sharma, S.K.: 'A literature review of IGBT fault diagnostic and protection methods for power inverters', *IEEE Trans. Ind. Appl.*, 2009, **45**, (5), pp. 1770–1777